Regular Article

LYMPHOID NEOPLASIA

Bif-1 haploinsufficiency promotes chromosomal instability and accelerates *Myc*-driven lymphomagenesis via suppression of mitophagy

*Yoshinori Takahashi,[1] *Tsukasa Hori,[1] Timothy K. Cooper,[2] Jason Liao,[3] Neelam Desai,[1] Jacob M. Serfass,[1] Megan M. Young,[1] Sungman Park,[1] Yayoi Izu,[4] and Hong-Gang Wang[1,3]

[1]Department of Pharmacology, [2]Department of Comparative Medicine, [3]Hershey Cancer Institute, and [4]Department of Microbiology and Immunology, The Pennsylvania State University College of Medicine, Hershey, PA

Key Points
• *Bif-1* acts as a haploinsufficient tumor suppressor in *Myc*-induced lymphomagenesis.   • Bif-1 plays a key role in mitophagy to maintain chromosome stability.

Malignant transformation by oncogenes requires additional genetic/epigenetic changes to overcome enhanced susceptibility to apoptosis. In the present study, we report that *Bif-1* (*Sh3glb1*), a gene encoding a membrane curvature–driving endophilin protein, is a haploinsufficient tumor suppressor that plays a key role in the prevention of chromosomal instability and suppresses the acquisition of apoptosis resistance during *Myc*-driven lymphomagenesis. Although a large portion of *Bif-1*–deficient mice harboring an Eμ-*Myc* transgene displayed embryonic lethality, allelic loss of *Bif-1* dramatically accelerated the onset of *Myc*-induced lymphoma. At the premalignant stage, hemizygous deletion of *Bif-1* resulted in an increase in mitochondrial mass, accumulation of DNA damage, and up-regulation of the antiapoptotic protein Mcl-1. Consistently, allelic loss of *Bif-1* suppressed the activation of caspase-3 in *Myc*-induced lymphoma cells. Moreover, we found that Bif-1 is indispensable for the autophagy-dependent clearance of damaged mitochondria (mitophagy), because loss of *Bif-1* resulted in the accumulation of endoplasmic reticulum–associated immature autophagosomes and suppressed the maturation of autophagosomes. The results of the present study indicate that *Bif-1* haploinsufficiency attenuates mitophagy and results in the promotion of chromosomal instability, which enables tumor cells to efficiently bypass the oncogenic/metabolic pressures for apoptosis. (*Blood*. 2013;121(9):1622-1632)

Introduction

Tumorigenesis is a multistep process by which normal cells progressively accumulate genetic mutations and epigenetic modifications that allow for sustained cell proliferation. During this process, overproliferated precancerous cells are exposed to a variety of environmental stresses (eg, growth factor limitation and nutrient starvation) that induce apoptosis. Evasion of apoptosis is therefore widely acknowledged to be a critical step in tumor development and a hallmark of most types of cancers.[1]

The Bcl-2 family of proteins, which is composed of antiapoptotic (eg, Bcl-2, Bcl-xL, and Mcl-1), multidomain proapoptotic (eg, Bax and Bak), and BH3-only proapoptotic regulatory members, plays a central role in the modulation of outer mitochondrial membrane (OMM) permeabilization to regulate the activation of downstream caspases and apoptosis. Overexpression of the antiapoptotic Bcl-2 family members or deletion of the proapoptotic members has been shown to synergize oncogene-driven tumorigenesis.[2] Moreover, recent high-resolution somatic copy-number alterations analyses across multiple cancer types have revealed that human cancer cells frequently amplify *Bcl-xL-* and *Mcl-1*–containing regions and depend on the expression of these antiapoptotic genes for survival.[3]

Macroautophagy, hereafter referred as autophagy, is a lysosome-mediated intracellular degradation process for turnover of proteins and organelles. It has been shown that inhibition of autophagy by a lysosomal inhibitor enhances p53-mediated apoptosis and tumor regression in a *Myc* oncogene–induced mouse lymphoma model.[4] Moreover, autophagy facilitates cancer cell survival by maintaining functional mitochondria to support tumor development during oncogenic Ras activation.[5] Elevated levels of autophagy were also observed in tumor xenograft models,[6,7] supporting the notion that autophagy functions to promote tumor survival in response to exposure to metabolic stresses. Paradoxically, however, the induction of autophagy is generally suppressed or limited in many tumor tissues through mechanisms such as the haploid deletion of the autophagy-related gene *Beclin 1* or constitutive activation of the PI3K/MTOR signaling pathway.[8] Moreover, allelic loss of *Beclin 1* has been shown to promote spontaneous or *Myc* oncogene–induced tumorigenesis in mice.[9,10] Furthermore, inhibition of autophagy in Bcl-2–overexpressing, apoptosis-incompetent cells has been shown to result in the accumulation of polyubiquitinated proteins and damaged mitochondria that promote the production of reactive oxygen species and chromosomal instability.[11,12] Therefore,

although the prosurvival function of autophagy for cancer cell growth often overwhelms the tumorigenic effects of autophagy deficiency,[9] defects in autophagy in certain circumstances may promote tumorigenesis.

Bif-1 (SH3GLB1/Endophilin B1), a member of the membrane curvature–driving endophilin family of proteins, regulates the induction of apoptosis and autophagy.[13] In humans, *Bif-1* is located on chromosome 1p22, a region that is frequently deleted in neoplasms.[14] Down-regulation of *Bif-1* expression has been reported in a variety of cancers.[15-19] We reported previously that knockdown of *Bif-1* enhances the tumorigenicity of HeLa cells in vivo[20] and the targeted deletion of *Bif-1* promotes spontaneous tumor development in mice.[21] Although these studies highlight the importance of Bif-1 as a tumor suppressor, the mechanism behind the promotion of tumorigenesis by *Bif-1* deficiency remains unclear. In the present study, we provide evidence that Bif-1 regulates autophagy-dependent mitochondrial turnover and acts as a haploinsufficient tumor suppressor to prevent chromosomal instability and the acquisition of apoptosis resistance during *Myc*-driven lymphomagenesis.

Methods

Mice

C57BL/6J wild-type mice and B6.Cg-Tg(IghMyc)22Bri/J (Eµ-*Myc*) mice were purchased from The Jackson Laboratory. All animal protocols were approved by the Pennsylvania State University Animal Care and Use Committee. B6.*Bif-1*$^{+/-}$ and B6.*Bif-1*$^{-/-}$ female mice were generated by backcrossing B6/129.*Bif-1*$^{-/-}$ mice[20] with C57BL/6J wild-type mice for 12 generations and intercrossed with Eµ-*Myc* transgenic male mice. PCR-based genotyping is described in supplemental Methods (available on the *Blood* Web site; see the Supplemental Materials link at the top of the online article).

Flow cytometry and karyotype analyses

Splenocytes were prepared from prelymphomatous mice. The cells were stained with 100nM MitoTracker Green FM (M-7514; Invitrogen) for 30 minutes and analyzed using an LSR II Flow Cytometer System (BD Biosciences) and FlowJo Version 9.3.2 software (TreeStar). For karyotype analyses, the cells were treated with 5 µg/mL of lipopolysaccharide overnight to stimulate cell-cycle progression. Metaphase spreads were then prepared using standard procedures after 10 µg/mL of Colcemid (KaryoMax, 15212-012; Invitrogen) treatment for 2 hours. Each metaphase was evaluated for chromosomal aneuploidy. The total number of chromosomes in each metaphase was counted from photographs.

Electron microscopy

Cells seeded on Thermanox plastic coverslips (72280; Electron Microscopy Sciences) were treated with 30µM carbonyl cyanide 3-chlorophenylhydrazone (CCCP) or DMSO for 24 hours and then fixed in Karnovsky fixative (1.5% paraformaldehyde/3% glutaraldehyde in 0.1M cacodylate buffer, pH 7.3) containing 4.2mM ethyleneglycol-bis(b-aminoethyl)-N,N,N′,N′-tetracetic acid for 30 minutes at room temperature, followed by 2 hours at 4°C. The cells were postfixed in 1% osmium tetroxide/1.5% potassium ferrocyanide in 0.1M sodium cacodylate, pH 7.3, for 30 minutes at 4°C, soaked in 1% uranyl acetate for 2 hours, dehydrated in a graded series of ethanol, embedded in EMbed 812 resin (14120; Electron Microscopy Sciences), and sectioned at a thickness of 70-90 nm. The sections were mounted on mesh copper grids, stained with aqueous uranyl acetate and lead citrate, and analyzed using a JEM 1400 transmission electron microscope (JEOL).

Results

Bif-1 haploinsufficiency accelerates *Myc*-driven lymphomagenesis

To further explore the potential of *Bif-1* as a tumor suppressor, *Bif-1*$^{+/-}$ mice with a C57BL/6J genetic background were crossed with Eµ-*Myc* transgenic mice, a well-established model for mouse B-cell lymphoma.[22] We found that knockout of *Bif-1* accelerated Eµ-*Myc*–induced tumor onset and mortality compared with Eµ-*Myc/Bif-1*$^{+/+}$ mice (median onset, 65 vs 107 days, respectively, *P* = .0006; Figure 1A). Eµ-*Myc/Bif-1*$^{+/-}$ mice also exhibited a shortened life span compared with Eµ-*Myc/Bif-1*$^{+/+}$ mice (median onset, 75 days, *P* < .0001). Although 36.5% of Eµ-*Myc/Bif-1*$^{+/+}$ mice (19 of 52) survived more than 135 days, none of the Eµ-*Myc/Bif-1*$^{+/-}$ (0 of 53) or Eµ-*Myc/Bif-1*$^{-/-}$ (0 of 9) mice did. No statistically significant difference in disease onset or mortality was observed between Eµ-*Myc/Bif-1*$^{+/-}$ and Eµ-*Myc/Bif-1*$^{-/-}$ mice. Eµ-*Myc/Bif-1*$^{+/+}$ and Eµ-*Myc/Bif-1*$^{+/-}$ mice were born at the expected Mendelian ratio and appeared healthy at birth (data not shown). Similarly, newborn Eµ-*Myc/Bif-1*$^{-/-}$ mice appeared normal and indistinguishable from their wild-type littermates. However, although *Bif-1*$^{-/-}$ mice without the Eµ-*Myc* transgene were born at normal Mendelian ratios,[20] the frequency of birth of Eµ-*Myc/Bif-1*$^{-/-}$ mice was significantly lower than expected (eg, 9.8% vs 25.0% in Eµ-*Myc/Bif-1*$^{+/-}$ and *Bif-1*$^{-/-}$ matings; supplemental Table 1). To determine whether a portion of Eµ-*Myc/Bif-1*$^{-/-}$ mice die during embryogenesis, embryos were dissected at several developmental stages. We found few Eµ-*Myc/Bif-1*$^{-/-}$ embryos with no apparent developmental defects in addition to several resorbed embryos at embryonic days 12.5 (E12.5) and E14.0 (supplemental Figure 1 and data not shown). A higher proportion of Eµ-*Myc/Bif-1*$^{-/-}$ embryos were detected at E9.5, although 2 of 5 isolated deciduae already contained developmentally arrested or resorbed Eµ-*Myc/Bif-1*$^{-/-}$ embryos. Therefore, we conclude that the majority of Eµ-*Myc/Bif-1*$^{-/-}$ mice die during embryogenesis, presumably around E9.5. These results indicate that not only does the loss of *Bif-1* promote embryonic lethality in Eµ-*Myc* transgenic mice, but *Bif-1* also functions as a haploinsufficient tumor suppressor gene in Eµ-*Myc*–induced lymphomagenesis.

During the course of monitoring lymphoma development, we found that a significant portion of Eµ-*Myc/Bif-1*$^{+/-}$ mice displayed the signs of lymphoma, including hunched posture, ruffled fur, slow movement, and labored breathing, without developing palpable swollen lymph nodes. Pathologic analysis revealed that the thymi in these mice were abnormally enlarged despite the absence of massive enlargement of lymph nodes (Figure 1B). Statistical analyses revealed that the frequency of thymic lymphoma observed in Eµ-*Myc/Bif-1*$^{+/-}$ mice was significantly higher than in Eµ-*Myc/Bif-1*$^{+/+}$ mice (33.3% vs 10.0%, respectively), suggesting that allelic loss of *Bif-1* affects proper lymphoblast homing. Increased frequency of thymic lymphoma was also observed in Eµ-*Myc/Bif-1*$^{-/-}$ mice (25.0%). Differences in the frequency of thymic lymphoma between Eµ-*Myc/Bif-1*$^{+/+}$ and Eµ-*Myc/Bif-1*$^{-/-}$ mice did not reach statistical significance; however, this may be attributable to the decreased survival and thus lower availability of Eµ-*Myc/Bif-1*$^{-/-}$ mice. The majority of all Eµ-*Myc* mice, regardless of *Bif-1* status, had developed splenomegaly at the onset of disease (Figure 1C). In addition, histological analyses showed that there were no obvious morphological differences among the lymphomatous spleens (data not shown).
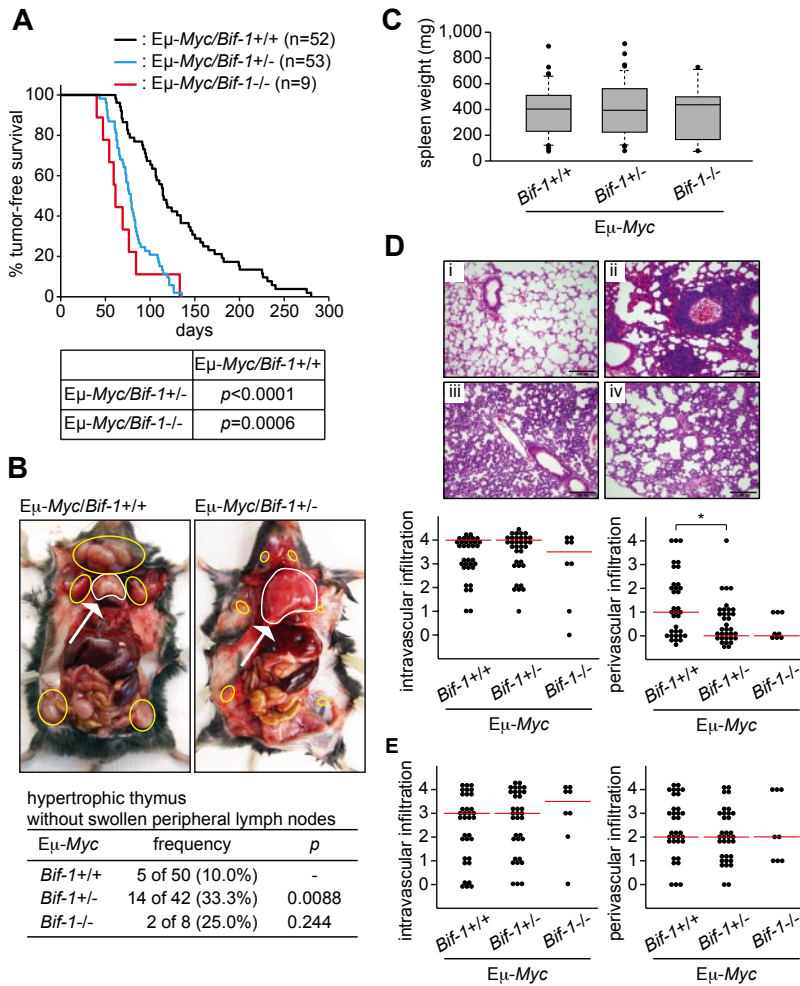
Figure 1. Loss of *Bif-1* promotes *Myc*-driven lymphoma development. (A) Kaplan-Meier tumor-free survival of Eμ-*Myc/Bif-1*^{+/+} (n = 52; median onset, 107 days), Eμ-*Myc/Bif-1*^{+/−} (n = 53; median onset, 75 days), and Eμ-*Myc/Bif-1*^{−/−} (n = 9; median onset, 65 days) mice is shown. Statistical significance was determined using a log-rank test. (B) *Bif-1* haploinsufficiency enhances the frequency of thymic lymphoma in Eμ-*Myc*–transgenic mice. Gross images of typical lymphomatous Eμ-*Myc/Bif-1*^{+/+} and Eμ-*Myc/Bif-1*^{+/−} mice with thymic lymphoma are shown. The lymph nodes and thymus are outlined by yellow circles and a white circle/arrow, respectively. Statistical significance was determined using a Fisher exact test. (C) The weights of spleens from all of the mice used in this figure were measured at the onset of lymphoma and are shown as a box plot. The lines, boxes, and error bars represent median values, 25-75 percentiles, and the 10-90 percentiles, respectively. (D-E) Allelic loss of *Bif-1* suppresses lung perivascular tumor formation in Eμ-*Myc*–transgenic mice. The lungs (D) and livers (data not shown) from lymphomatous Eμ-*Myc/Bif-1*^{+/+} (n = 34; ii), Eμ-*Myc/Bif-1*^{+/−} (n = 38; iii), Eμ-*Myc/Bif-1*^{−/−} (n = 8; iv), and control *Bif-1*^{+/+} mice (i) were stained with H&E. The degree of lymphoblast infiltration to pulmonary alveolar septa (D) or hepatic sinusoids (E) and perivascular interstitial stroma expanded by lymphoblasts (D-E) were scored as follows: 0 = normal; 1 = < 5%; 2 = 6%-15%; 3 = 16%-40%; and 4 = > 40%. The lines represent median values. Statistical significance was determined using a 2-way ANOVA followed by a Scheffe posthoc test. *$P < .05$.

Infiltration of lymphoblasts to the lung and the liver is frequently observed in lymphomatous Eμ-*Myc*–transgenic mice.[22] Consistently, thickened alveolar septa infiltrated with blast cells were observed in the lungs of *Bif-1*^{+/+} mice harboring the Eμ-*Myc* transgene (Figure 1D). Similar levels of blast cell infiltration were detected in the intravascular compartments of lungs isolated from lymphomatous Eμ-*Myc/Bif-1*^{+/−} and Eμ-*Myc/Bif-1*^{−/−} mice. However, significant inhibition of perivascular clustering of blast cells in the lung was observed in mice lacking 1 *Bif-1* allele, suggesting that Bif-1 regulates lymphoblast infiltration to certain types of tissues. In contrast, tumor infiltration in both the intravascular and perivascular regions of the liver was not affected by hemizygous or homozygous deletion of *Bif-1* (Figure 1E).

Bif-1 haploinsufficiency results in the up-regulation of Mcl-1 and suppresses caspase-3 activation in Eμ-*Myc*–induced lymphomatous lymph nodes

To determine whether the suppression of apoptosis is the mechanism by which *Bif-1* deficiency accelerates Eμ-*Myc*-induced lymphomagenesis, axillary lymph nodes were collected after the onset of lymphoma and activation of caspase-3 was determined by monitoring caspase-3 processing. As shown in Figure 2A and B, hemizygous or homozygous deletion of *Bif-1* significantly suppressed caspase-3 processing in lymphomatous lymph nodes. Similar results were obtained by immunohistochemical analyses (Figure 2C). In contrast, the expression of proliferating cell nuclear

antigen was not affected by loss of *Bif-1* (Figure 2D), suggesting that the suppression of apoptosis, rather than enhanced cell proliferation, is a mechanism through which the haplodeficiency of *Bif-1* promotes Eμ-*Myc*–induced lymphomagenesis. In agreement with these data, we showed previously that stable knockdown of *Bif-1* delays mitochondrial apoptosis and enhances the tumorigenicity of HeLa cells without affecting their proliferation rate.[20]

Inactivation of the ARF-MDM2-p53 pathway or dysregulation of antiapoptotic Bcl-2 family proteins are frequently observed in lymphomatous Eμ-*Myc*–transgenic mice[23,24] and thus are believed to be major contributors for *Myc*-driven tumorigenesis. Therefore, we next examined the expression profiles of these apoptosis-related proteins in lymphomatous tumors. Consistent with previous studies,[23,24] up-regulation of ARF and Bcl-xL was detected in Eμ-*Myc/Bif-1*^{+/+} tumors compared with normal lymph nodes obtained from control wild-type mice (Figure 2A). For all tumors tested, up-regulation of p53 was rarely observed. Although the Myc-induced suppression of Bcl-2 is reportedly disabled during lymphomagenesis,[24] the expression levels of Bcl-2 in the lymphomatous lymph nodes remained low compared with the control wild-type mouse lymph nodes. Despite significant reduction of caspase-3 processing, the expression levels of these antiapoptotic proteins in Eμ-*Myc/Bif-1*^{+/−} and Eμ-*Myc/Bif-1*^{−/−} tumors were comparable to those in Eμ-*Myc/Bif-1*^{+/+} tumors (Figure 2A-B). Interestingly, however, loss of *Bif-1* significantly enhanced the expression of Mcl-1, another member of the antiapoptotic Bcl-2 protein family. Furthermore, the Eμ-*Myc*–induced down-regulation of p62, an autophagic adaptor protein that mediates cell

Figure 2. *Bif-1* **haploinsufficiency up-regulates Mcl-1 expression and suppresses caspase-3 activation in** Eμ*-Myc*–**induced tumors.** Lymphomatous axillary lymph nodes were extirpated from each Eμ-*Myc*–transgenic mouse at the onset of disease. (A) Tissue lysates were prepared using a Tissuemiser homogenizer and analyzed by immunoblotting using the indicated antibodies. Representative blots of Eμ-*Myc/Bif-1*^{+/+} (n = 37), Eμ-*Myc/Bif-1*^{+/–} (n = 38), and Eμ-*Myc/Bif-1*^{–/–} (n = 8) tumors in addition to control *Bif-1*^{+/+} and *Bif-1*^{+/–} lymph nodes are shown. (B) The intensity of cleaved-Caspase-3 (C-Casp-3, p17), Mcl-1, and p62 were quantified by densitometry using Quantity One software and are shown as a box plot. To compare the signal intensities between the different gels, the intensity of each blot was adjusted to the value of untreated wild-type mouse embryonic fibroblast lysates, which were loaded on every gel. Statistical significance was determined using 2-way ANOVA followed by the Scheffe posthoc test. *$P < .05$. (C-D) Tissues subjected to immunohistochemical analyses using the indicated antibodies. The number of proliferating cell nuclear antigen (PCNA)–positive cells per field (400$\times$) was counted using a light microscope and is shown as a box plot in panel D. A total of 7451, 7251, and 9947 PCNA^{+} cells were counted from 3 Eμ-*Myc/Bif-1*^{+/+}, 3 Eμ-*Myc/Bif-1*^{+/–}, and 4 Eμ-*Myc/Bif-1*^{–/–} mice, respectively.
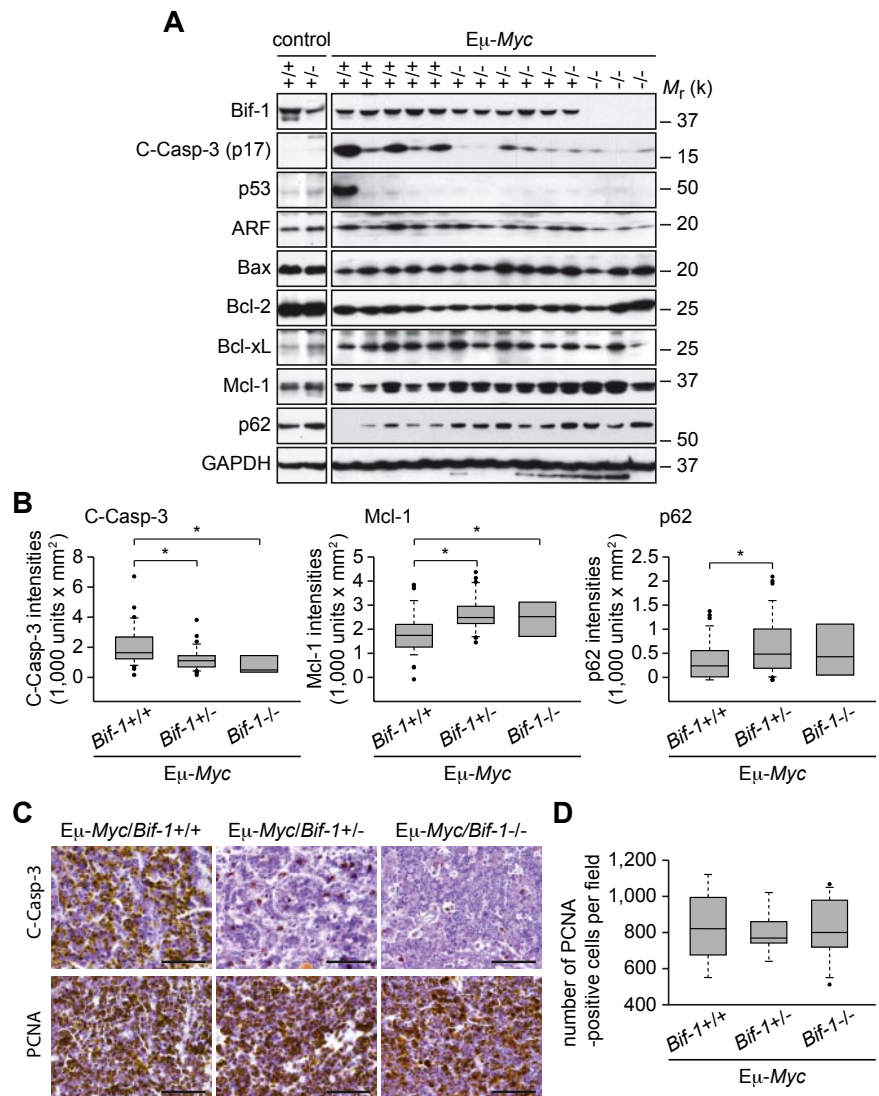
survival and cytoprotective stress-response pathways, was significantly suppressed by deletion of a *Bif-1* gene, supporting previous reports that *Bif-1* loss suppresses autophagy.[21,25,26] Because overexpression of Myc has been shown to induce autophagy[27] and p62 is an autophagic substrate, inhibition of an efficient autophagic degradation may be responsible for the sustained expression of p62 in lymphomatous tumors in Eμ-*Myc/Bif-1*^{+/–} and Eμ-*Myc/Bif-1*^{–/–} mice.

Bif-1 haploinsufficiency promotes chromosomal instability during *Myc*-induced neoplastic transformation

To determine whether *Bif-1* haploinsufficiency suppresses premalignant tumor cell death under the selection pressure, prelymphomatous Eμ-*Myc* mouse spleens in which overproliferated, yet not malignant, polyclonal lymphoblasts are predominantly present,[28] were extirpated before the onset of disease and subjected to immunoblot analyses. We detected a slight activation of caspase-3 in prelymphomatous Eμ-*Myc/Bif-1*^{+/+} cells compared with control splenocytes isolated from age-matched *Bif-1*^{+/+} mice (Figure 3A). Allelic loss of *Bif-1* did not suppress, but rather enhanced, caspase-3 cleavage in prelymphomatous Eμ-*Myc* splenocytes despite the increased levels of antiapoptotic Bcl-xL and Mcl-1 proteins detected in these cells.

Inhibition of autophagy by allelic loss of *Beclin 1* or homozygous deletion of *Atg5* promotes metabolic stress–induced chromosomal

instability and mammary tumorigenesis.[29] Because Myc activation induces autophagy[27] and allelic loss of *Bif-1* significantly increased p62 expression (Figure 2B), the elevated expression of antiapoptotic proteins in prelymphomatous Eμ-*Myc/Bif-1*^{+/–} cells may be caused indirectly by enhanced accumulation of genomic damage. To determine whether *Bif-1* haploinsufficiency promotes the induction of DNA damage during *Myc*-driven lymphomagenesis, we first examined the accumulation of γ-H2AX, a well-established DNA double-strand break marker. A strong accumulation of γ-H2AX signals was detected in prelymphomatous Eμ-*Myc/Bif-1*^{+/–} spleens (Figure 3A). Furthermore, a slight accumulation of γ-H2AX expression was detected in *Bif-1*^{–/–} spleens in the absence of the Eμ-*Myc* transgene, suggesting that *Bif-1* deficiency itself leads to the induction of DNA damage.

To determine whether the enhanced DNA double-strand breaks present in *Bif-1*–deficient cells leads to chromosomal aberrations, we next analyzed the karyotypes of splenocytes prepared from prelymphomatous Eμ-*Myc* mouse spleens. Consistent with the γ-H2AX data (Figure 3A), the frequency of aneuploidy induced by *Myc* was significantly increased by hemizygous and homozygous deletion of *Bif-1* (Figure 3B-C). Although the aneuploidy observed in Eμ-*Myc/Bif-1*^{+/+} splenocytes was accompanied by the deletion of chromosomes, a large portion of Eμ-*Myc/Bif-1*^{+/–} splenocytes
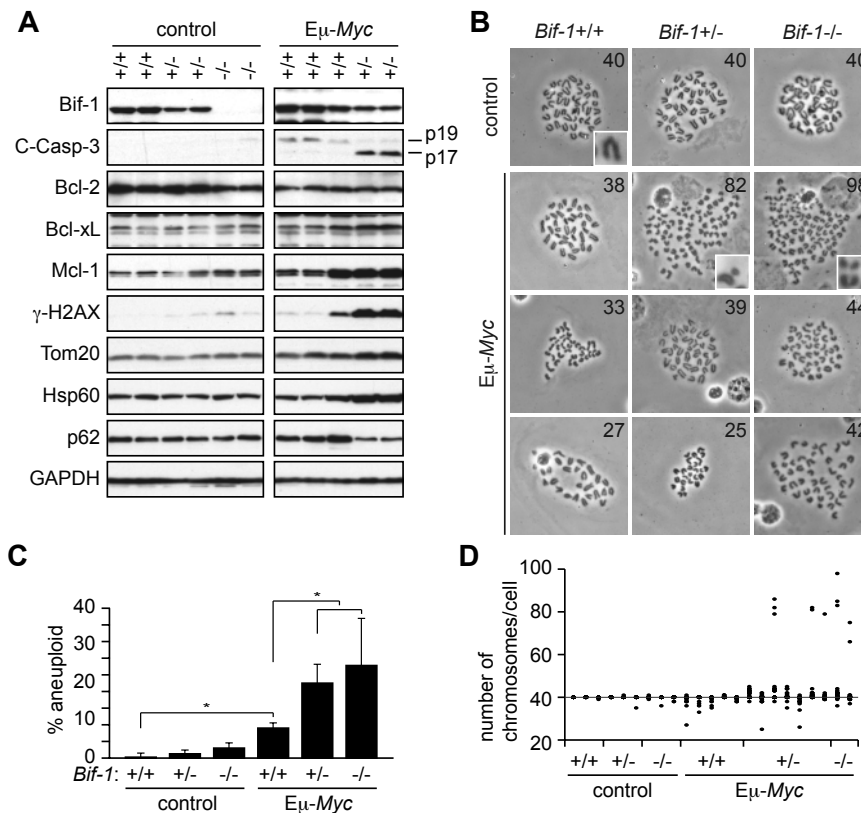
Figure 3. Bif-1 haploinsufficiency promotes Myc-induced genomic instability in prelymphomatous splenocytes. Spleens were isolated from 9-week-old prelymphomatous Eμ-Myc–transgenic and age-matched control mice with the indicated Bif-1 alleles. (A) Tissue lysates were subjected to immunoblot analyses using the indicated antibodies. (B-C) The karyotypes of Bif-1^{+/+} (n = 151 from 3 mice), Bif-1^{+/−} (n = 153 from 3 mice), Bif-1^{−/−} (n = 154 from 3 mice), Eμ-Myc/Bif-1^{+/+} (n = 268 from 5 mice), Eμ-Myc/Bif-1^{+/−} (n = 384 from 7 mice), and Eμ-Myc/Bif-1^{−/−} (n = 127 from 2 mice) splenocytes were analyzed. At least 50 metaphases were evaluated for each mouse. Representative images and magnified images of chromosomes are shown in panel B and the insets in panel B, respectively. The percentage of aneuploidy and the number of chromosomes per cell are shown in panels C (mean ± SD) and D, respectively. Statistical significance was determined using a Wilcoxon rank-sum test with continuity correction. *P < .01.

(32 of 43 aneuploid cells) and Eμ-Myc/Bif-1^{−/−} splenocytes (22 of 23 aneuploid cells) contained amplified numbers of chromosomes that were frequently accompanied by double-minute chromosomes (Figure 3B and D). No statistical significance in the rate of aneuploidy was observed between Eμ-Myc/Bif-1^{+/−} and Eμ-Myc/Bif-1^{−/−} mice. These results demonstrate that Bif-1 haploinsufficiency promotes chromosomal instability during Eμ-Myc–induced lymphomagenesis.

### Bif-1 haploinsufficiency results in the accumulation of mitochondria in prelymphomatous Eμ-Myc cells

In addition to enhanced DNA damage induction, a negative correlation between expression of Bif-1 and accumulation of mitochondrial marker proteins (Tom20, a major component of the translocase of OMM complex and Hsp60, a mitochondrial matrix chaperonin) was also detected in the prelymphomatous Eμ-Myc transgenic spleen (Figure 3A). To determine whether Bif-1 haploinsufficiency promotes mitochondrial accumulation during Myc-induced neoplastic transformation, prelymphomatous splenocytes were isolated from littermates of Eμ-Myc/Bif-1^{+/−} and Bif-1^{+/+} matings. Histological analyses revealed that the distinction between the red and white pulps was largely lost and monotonous plasmacytoid cells had accumulated in both Bif-1^{+/+} and Bif-1^{+/−} spleens in the presence of an Eμ-Myc gene (Figure 4A), indicating that Bif-1 homozygosity is not required for Myc-induced overproliferation at the premalignant stage. The Myc-induced increase in intensity of the mitochondrial dye MitoTracker Green FM was further enhanced on hemizygous deletion of Bif-1 (Figure 4B-C). Similar results were obtained using another pair of littermates (Figure 4D). Furthermore, electron microscopic analyses showed that mitochondrial mass was indeed increased by Bif-1–hemizy-

gous deletion (Figure 4E-F). Swollen mitochondria were occasionally observed in Eμ-Myc/Bif-1^{+/−} cells (red arrows in Figure 4E). These results clearly indicate that Bif-1 is required for the maintenance of proper mitochondrial mass during Myc-induced lymphomatous transformation.

Loss of Bif-1 abrogates mitochondrial clearance by autophagy

Autophagy is the central process for the maintenance of mitochondrial quality and quantity.[30] To determine whether Bif-1 is responsible for the degradation of mitochondria, we took advantage of the Parkin-overexpression system, followed by treatment with a mitochondrial uncoupler, CCCP, a system that is widely used to study autophagy-dependent clearance of damaged mitochondria.[31] After treatment with the mitochondrial uncoupler, the E3-ubiquitin ligase Parkin translocates from the cytosol to mitochondria, where it mediates the ubiquitination of a variety of OMM proteins to promote autophagic clearance of damaged mitochondria.[30] After treatment with CCCP, mitochondria labeled with MitoTracker CMTMRos were fragmented and accumulated in the perinuclear region of myc-Parkin–expressing cells regardless of the expression of Bif-1 (Figure 5A). Although a significant portion of myc-Parkin/Bif-1^{+/+} cells partially or completely lost mitochondrial signals after 24 hours of treatment with CCCP, such a reduction of mitochondria was not observed in cells lacking Bif-1. Consistent with these observations, we found that both endogenous Tom20 and Hsp60 signals were fragmented and accumulated in the perinuclear region of both mCherry-Parkin/Bif-1^{+/+} and mCherry-Parkin/Bif-1^{−/−} cells after 6 hours of treatment with CCCP (supplemental Figure 2). Moreover, both Tom20 and Hsp60 signals were partially or completely lost in Parkin-overexpressing wild-type cells after 24 hours of CCCP treatment (Figure 5B). We also

Figure 4. *Bif-1* haploinsufficiency results in an increase in mitochondrial mass at premalignant stage of *Myc*-induced lymphoma. Prelymphomatous spleens were isolated from male littermate mice at the age of 12 weeks (panels A-C and E-F) and 10 weeks old (panel D). (A) Tissues were divided into 2 parts and a portion processed for electron microscopic analysis was stained with methylene blue and Azure II. (B) Splenocytes were prepared from another half portion of tissue, stained with MitoTracker Green FM for 30 minutes, and analyzed by flow cytometry. The percentages of cells with increased numbers of mitochondria by Myc are shown. (C-D) Geometric means of MitoTracker Green FM signals quantified and shown as relative intensities. (E) Tissue blocks in panel A were sectioned and analyzed by electron microscopy. The scale bars represent 1 μm. (F) Total mitochondrial area per cytoplasmic area in Eμ-*Myc/Bif-1*$^{+/+}$ (n = 136) and Eμ-*Myc/Bif-1*$^{+/-}$ (n = 129) cells in panel E was quantified using ImageJ software and is shown as a box plot. The lines, boxes, and error bars represent median values, 25-75 percentiles, and 10-90 percentiles, respectively. Statistical significance was determined using a Wilcoxon rank-sum test with continuity correction. *$P < .0001$.
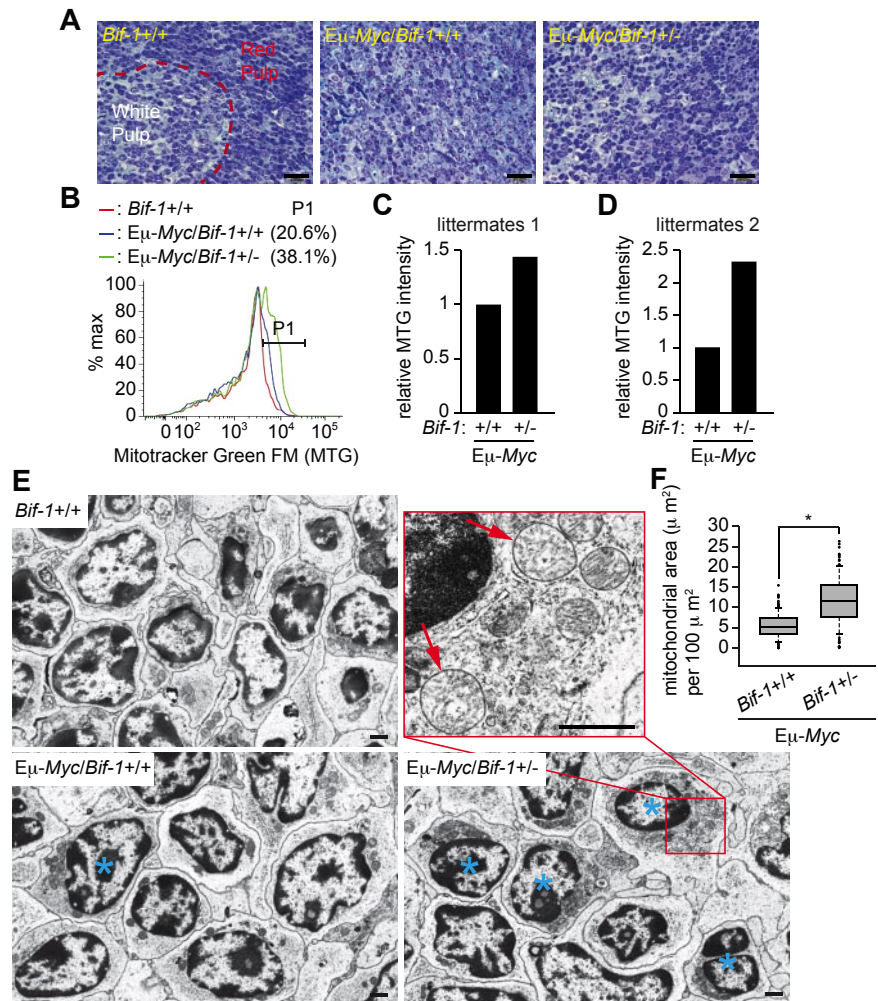
found that *Bif-1* loss abrogated CCCP-induced reduction of Hsp60, but not Tom20 signals. Similarly, Bif-1–dependent degradation of Hsp60, but not Tom 20, was detected in Parkin-overexpressing cells after treatment with CCCP, as shown by immunoblot analysis (Figure 5C). The decreased expression of mitochondrial proteins was restored 96 hours after the treatment, suggesting that mitochondria were regenerated. The inhibition of Parkin-dependent degradation of mitochondrial matrix markers in Bif-1–deficient cells was completely rescued by the restoration of Bif-1 expression (Figure 5D and supplemental Figure 3A). Because Parkin promotes the autophagy-independent degradation of OMM proteins through the ubiquitin-proteasome system after treatment with CCCP,[32-34] these results clearly indicate that Bif-1 specifically regulates mitochondrial degradation through autophagy. Because Bif-1 is also known to accumulate in mitochondria on the induction of mitochondrial apoptosis[20,35] and CCCP-induced mitochondrial degradation in mouse embryonic fibroblasts is dependent on Parkin[32] (supplemental Figure 3B), Bif-1 may play a role in the mitochondrial translocation of Parkin on CCCP treatment. However, mitochondrial signals were extensively colocalized with mCherry-Parkin regardless of Bif-1 expression in response to CCCP (white arrows in supplemental Figure 2), thus suggesting that Bif-1 acts downstream of Parkin to regulate autophagy-dependent mitochondrial clearance (mitophagy).

To gain further insight in the role of Bif-1 on mitophagy, *myc-Parkin/Bif-1*$^{-/-}$ cells transduced with Bif-1-AcGFP– and mito-mCherry–encoding lentiviruses were treated with CCCP and subjected to time-lapse fluorescence microscopic analyses. Consistent with our previous study,[26] Bif-1 signals were detected diffusely in the cytoplasm in addition to the juxtanuclear region, but not at the mitochondria (data not shown). After treatment with CCCP, Bif-1 signals were time dependently accumulated on portions of fragmented and perinuclear-clustered mitochondria (Figure 6A). The signal intensities of Bif-1$^+$ mitochondria were decreased over the incubation time period, suggesting that these structures were eventually degraded. Furthermore, short-interval imaging showed that Bif-1 strongly associated with fragmented mitochondria (Figure 6B). Some of the Bif-1$^+$ mitochondria was colocalized with LC3 (Figure 6C-D), supporting the notion that Bif-1 regulates the autophagy-dependent clearance of mitochondria. To investigate this further, we next examined whether *Bif-1* loss can also affect mitochondrial quantity control under ischemic condition, a physiologically relevant stress. Consistent with the data obtained from prelymphomatous Eμ-*Myc* splenocytes (Figure 3A), enhanced accumulation of mitochondrial markers and reduced degradation of p62 were observed in *Bif-1*$^{-/-}$ cells after exposure to hypoxic and low-nutrient conditions (supplemental Figure 4). Moreover, the induction of H2AX phosphorylation was enhanced by *Bif-1* deficiency, also suggesting that Bif-1–mediated mitophagy may contribute to the suppression of DNA damage during metabolic stress.
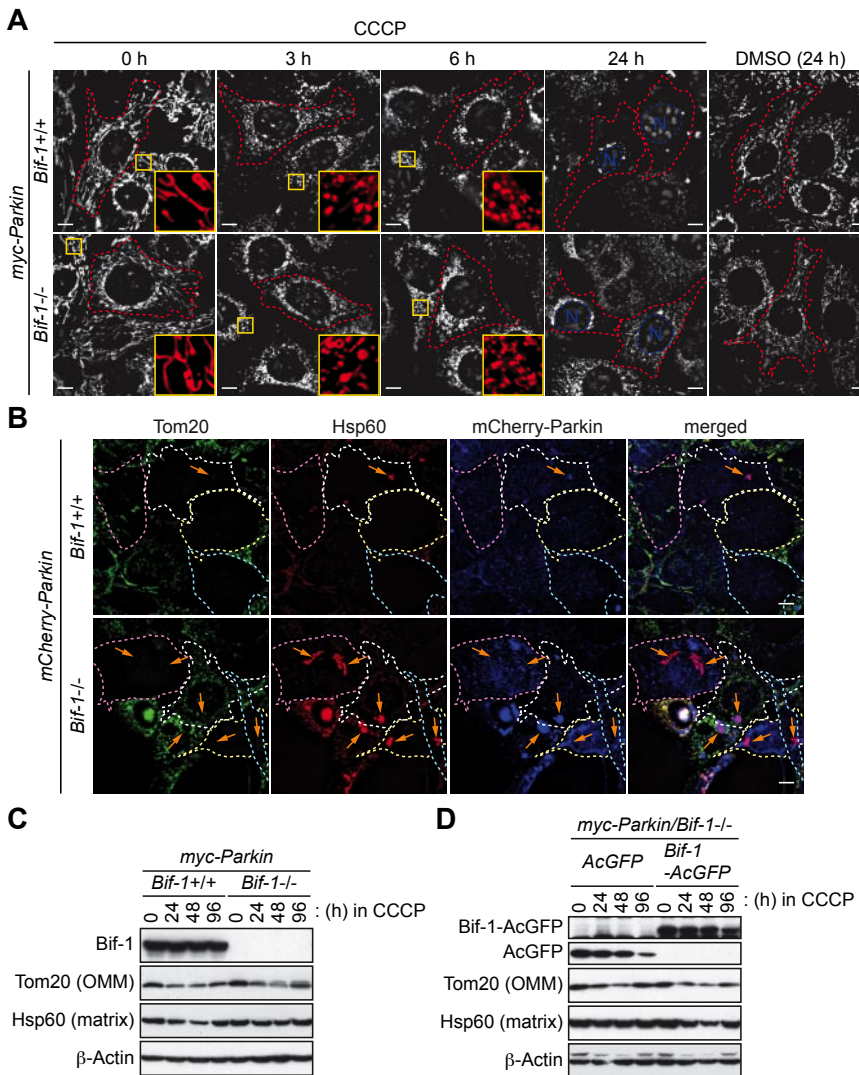
Figure 5. Loss of *Bif-1* suppresses mitophagy. *Bif-1*^{+/+} and *Bif-1*^{−/−} mouse embryonic fibroblasts were transduced with lentiviruses encoding myc-Parkin or mCherry-Parkin and selected with puromycin for 5 days. (A) The resultant stable clones were prestained with MitoTracker CMTMRos, treated with 30μM CCCP or control DMSO for the indicated periods of time, and analyzed by fluorescent microscopy. Magnified images are shown in the insets. (B) Cells were treated with 30μM CCCP for 0, 6, and 24 hours and immunostained for Tom20 and Hsp60. Data shown are representative of the 24-hour time point; images at the 0- and 6-hour time points are shown in supplemental Figure 2. Arrows represent Hsp60^{+} and Tom20^{−} structures. (C-D) Cells treated with 30μM CCCP for the indicated periods of time were subjected to immunoblot analysis using the indicated antibodies. The scale bars in panels A and B represent 10 μm.

Bif-1 regulates the maturation of nascent autophagosomes during mitophagy

Autophagy is initiated by the formation of isolation membranes (IMs)/phagophores that engulf cytoplasmic components and elongate, expand, and seal to form completed autophagosomes, which ultimately undergo maturation on fusion with endosomes and lysosomes for the degradation of the inner materials.[36,37] To determine the step at which loss of *Bif-1* suppresses mitophagy, Parkin-overexpressing cells were treated with CCCP for the indicated time periods and immunostained for Atg16L (IMs), LC3 (IMs and autophagosomes), and Lamp1 (lysosomes). As shown in supplemental Figure 5A and B, CCCP treatment induced the foci formation of Atg16L and LC3 in the close proximity of the clusters of Hsp60^{+} structures in wild-type cells. Lamp1 signals were also accumulated in close proximity to mitochondria, where they partially colocalized with LC3. Despite strong inhibition of mitochondrial loss, the CCCP-induced Atg16L and LC3 foci formation was not suppressed by knockout of *Bif-1*, indicating that Bif-1 is not required for the formation of nascent autophagosomes in response to CCCP treatment.

To further determine the effect of *Bif-1* loss on mitophagy, the cells were subjected to electron microscopic analysis. We found that although a large portion of mitochondria were lost in CCCP-treated *myc-Parkin/Bif-1*^{+/+} cells, degradative autophagic vacuole (Avd) and nascent or immature autophagosome (Avi)–like structures were readily observable in the cytoplasm of these cells (Figure 7Ai). In stark contrast, many fragmented mitochondria were accumulated in the perinuclear region of CCCP-treated *myc-Parkin/Bif-1*^{−/−} cells (Figure 7Aii). In agreement with a recent study,[32] a large portion of these fragmented mitochondria were accompanied by either a partially or completely ruptured OMM structure (Figure 7Aii and iii and supplemental Figure 6B) that was distinct from the double-membrane structure of control DMSO-treated mitochondria (supplemental Figure 6A). Statistical analysis revealed that loss of *Bif-1* significantly increased the number of total and ruptured mitochondria in the cytoplasm of CCCP-treated cells (Figure 7B), supporting our finding that Bif-1 is required for the autophagic clearance of damaged mitochondria. Consistent with the immunofluorescence data (supplemental Figure 5), the total number of CCCP-induced IM and Avi-like structures was not suppressed, but rather was slightly increased, by the loss of *Bif-1* (Figure 7C). The IM/Avi-like structures (black arrows in Figure 7Aiii and iv and supplemental Figure 6B) in CCCP-treated *myc-Parkin/Bif-1*^{−/−} cells were occasionally found to be associated with fragmented and/or ruptured mitochondria (double-arrowheads

Figure 6. CCCP induces Bif-1 and LC3 translocation to fragmented mitochondria. *myc-Parkin/Bif-1*^{−/−} mouse embryonic fibroblasts were transduced with lentiviruses encoding Bif-1–AcGFP and Mito-mCherry. (A-B) The cells were treated with 30μM CCCP for 4 hours (A) or 20 hours (B) and then analyzed by time-lapse fluorescent microscopy at 5-minute (A) or 1-minute (B) intervals. The time stamps delineate the incubation time periods in hours (°) and minutes (′) after the initiation of time-lapse imaging. (C) Cells treated with 30μM CCCP for 20 hours, immunostained for LC3, and analyzed by fluorescence deconvolution microscopy. Magnified images are shown in the insets. Arrows indicate colocalization of Bif-1–AcGFP, Mito-mCherry, and LC3. (D) The fluorescence intensities along the dotted line in panel D were quantified using SlideBook Version 5.0 software. The values of the vertical axis represent fluorescence intensity units (ADU). The horizontal axis represents distance (S indicates start point; and E, end point). The scale bars represent 10 μm in the left panels in panels A and B and 5 μm in the right panels of time-lapse images in panels A through C.
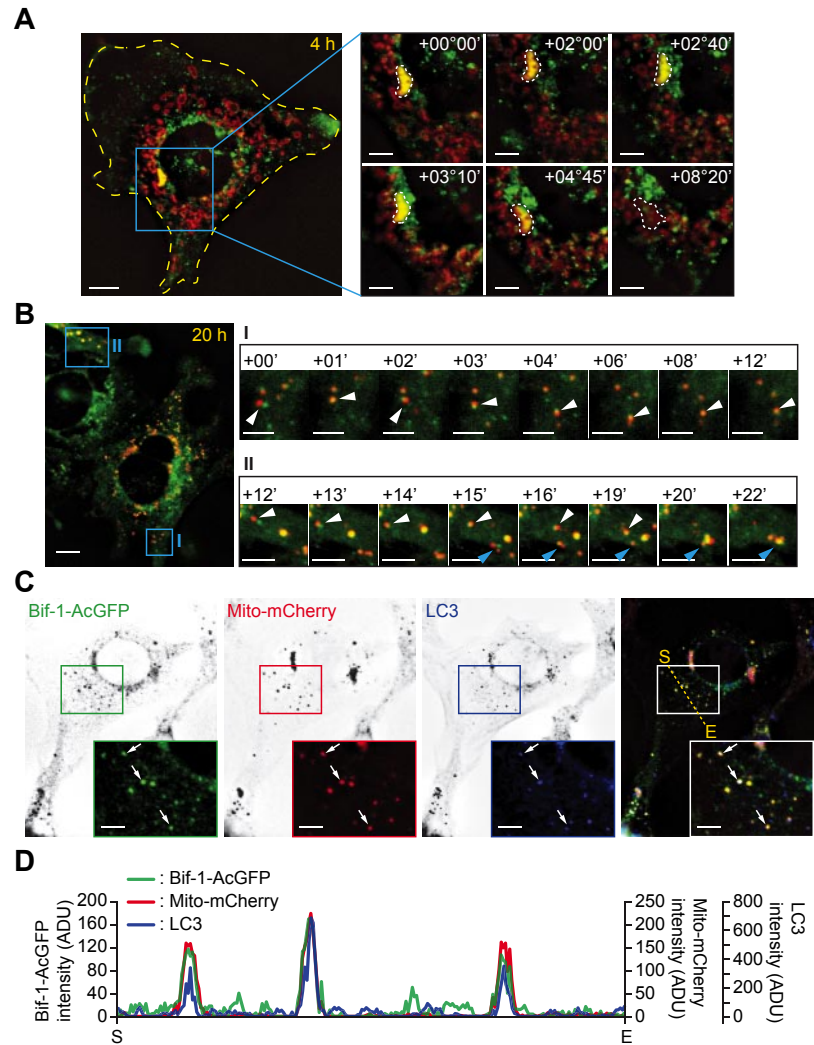
in Figure 7Aiii and iv and supplemental Figure 6B), although many of them remained associated with the endoplasmic reticulum (black arrowheads in Figure 7Aiii and iv and supplemental Figure 6B). Although numerous electron-dense lysosome-like structures were coaccumulated with ruptured mitochondria at the perinuclear region (Figure 7Aii and supplemental Figure 6B), the number of Avds was significantly reduced in *Bif-1*–deficient cells (Figure 7Av and D). These results suggest that Bif-1 regulates mitophagy by promoting the maturation of nascent autophagosomes.

Discussion

In the present study, we provide the evidence that *Bif-1* plays a key role in autophagy-dependent clearance of mitochondria and functions as a haploinsufficient tumor suppressor to prevent malignant transformation of Eμ-*Myc* transgenic pre-B cells. Our data show that *Bif-1* haploinsufficiency results in the attenuation of caspase-3 activation in Eμ-*Myc*^{+} lymphoma cells (Figure 2A-C). In agreement with this finding, Bif-1 was originally discovered as a Bax activator to promote mitochondrial apoptosis in response to a variety of cytotoxic stresses.[20,38] *Bax* loss has been shown to impair Myc-induced apoptosis and to accelerate Eμ-*Myc*–induced lymphomagenesis in mice.[39] Therefore, one can speculate that suppression of the Bax-mediated apoptotic pathway could be the mechanism behind the inhibition of Eμ-*Myc*–induced caspase-3 activation by allelic loss of *Bif-1*. However, our data in prelymphomatous Eμ-*Myc* transgenic spleens revealed that *Bif-1* haplodeficiency does not suppress, but rather promotes, caspase-3 activation (Figure 3A), suggesting that *Bif-1* loss itself may not be sufficient to suppress the induction of apoptosis in overproliferated prelymphomatous cells under oncogenic/metabolic stresses. In contrast, we found that *Bif-1* haploinsufficiency resulted in an increase in mitochondrial mass, the promotion of chromosomal instability, and the up-regulation of antiapoptotic proteins such as Mcl-1. Therefore, we propose that loss of *Bif-1* enables tumor cells to adapt to selection pressures by enhancing chromosomal instability and up-regulating antiapoptotic Bcl-2 family proteins. Alternatively, *Bif-1* haploinsufficiency may promote the survival of tumor cells through the up-regulation of proteins downstream of the mitochondrial pathway to inhibit the activity of cleaved mature caspases. Nonetheless, a significant reduction of cleaved caspase-3 accompanied by the up-regulation of Mcl-1 was observed in the majority of Eμ-*Myc*/*Bif-1*^{+/−} and Eμ-*Myc*/*Bif-1*^{−/−} cells after the onset of lymphoma, suggesting that attenuation of the mitochondrial pathway is likely a main cause of the acceleration of lymphomagenesis by *Bif-1* haploinsufficiency.
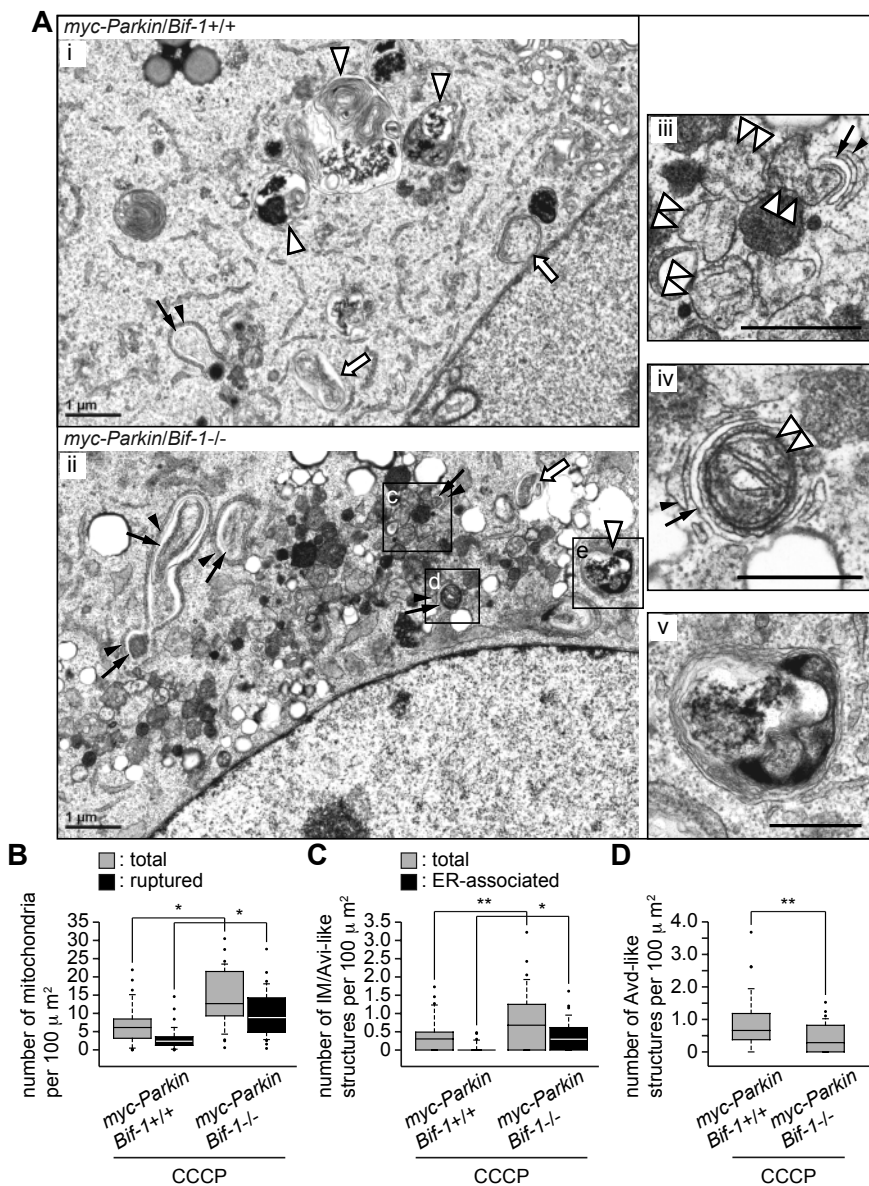
Figure 7. Bif-1 plays a key role in the maturation of nascent autophagosomes during mitophagy. myc-Parkin–expressing mouse embryonic fibroblasts were treated with 30μM CCCP for 24 hours and subjected to electron microscopic analysis. (A) Representative images of *Bif-1* wild-type and *Bif-1*–deficient cells are shown in subpanels i and ii. OMM-ruptured or OMM-preserved fragmented mitochondria that were closely associated with an isolation membrane are shown in subpanels iii and iv. An Avd-like structure observed in *Bif-1*–deficient cells is shown in subpanel v. Black arrowheads and arrows indicate endoplasmic reticulum (ER) membranes and ER-associated IMs, respectively. Open arrowheads, double-arrowheads, and arrows indicate Avd-like structures, fragmented mitochondria, and Avi-like structures, respectively. The scale bars represent 1 μm in subpanels i and ii and 0.5 μm in subpanels iii through v. The number of ruptured mitochondria and total mitochondria (OMM-ruptured and OMM-preserved; B), ER-associated IM/Avi-like structures and total IM/Avi-like structures (ER-associated and ER-nonassociated; C), and Avd-like structures (D) per cell were counted, normalized with cytoplasmic area (100 μm²) and are shown as box plots. The lines, boxes, and error bars represent median values, 25-75 percentiles, and 10-90 percentiles, respectively. Statistical significance was determined using a Wilcoxon rank-sum test with continuity correction. *$P < .0001$; **$P = .0227$ in panel C and $P = .0018$ in panel D.

Using Parkin-mediated mitophagy as a model, we also show in the present study that Bif-1 is required for autophagy-dependent clearance of damaged mitochondria. Because the accumulation of damaged mitochondria by impairment of autophagy results in the promotion of reactive oxygen species generation and DNA damage accumulation,[12] failure of proper mitochondrial clearance is likely the mechanism behind the promotion of chromosomal instability by *Bif-1* loss in *Myc*-induced lymphoma cells. However, we do not exclude the possibility that some other mechanisms may also contribute to *Bif-1* haploinsufficiency-induced chromosomal instability. Interestingly, a recent study has shown that UVRAG, which bridges Bif-1 association with Beclin 1,[21] regulates the activation of DNA-PK and promotes DNA double-strand-break repair in an autophagy-independent manner.[40] Further studies are warranted to determine whether Bif-1 also regulates chromosomal instability and tumorigenesis through an UVRAG-dependent and autophagy-independent mechanism.

Although we and others have previously reported that Bif-1 forms a complex with Beclin 1 through UVRAG to regulate autophagosome formation induced by nutrient starvation or in models of Parkinson disease,[21,25] the results of the present study showed that *Bif-1* loss does not suppress, but rather accumulates, the IMs and the Avi-like structures during CCCP treatment. It has been reported that UVRAG promotes autophagy, not only by interacting with the Beclin 1-Vps34 complex at the autophagosome formation stage,[41] but also by accelerating the maturation of endosomes and autophagosomes through the interaction with the c-Vps complex.[42] Indeed, we found herein that the number of Avd-like structures induced by CCCP was slightly but significantly reduced by the loss of *Bif-1* (Figure 7D). Many of the IMs/Avi-like structures observed in CCCP-treated *Bif-1*–deficient cells remained associated with the ER (Figure 7C). It has been shown previously that the IM, but not the completed autophagosome, frequently associates with the endoplasmic reticulum.[43,44] Therefore, in this scenario, Bif-1 may play a key role in the completion of nascent autophagosome formation during mitophagy.

Our results also unveiled unexpected roles of *Bif-1* in embryonic development and tumor cell homing in response to *Myc*

dysregulation. It has been reported that a fraction of Eμ-*Myc* transgenic mice overexpressing Mcl-1 (VavP-*Mcl-1*/Eμ-*Myc*) undergo perinatal lethality.[45] Moreover, in lymphomatous VavP-*Mcl-1*/Eμ-*Myc* mice, lymphoma cells were found to infiltrate and thicken the alveolar walls in the lungs, but not to accumulate in solid masses, a result similar to that observed by hemizygous deletion of *Bif-1* in Eμ-*Myc*–transgenic mice. Therefore, upregulation of Mcl-1 expression could be a mechanism behind the embryonic lethality and/or misregulated lymphoma cell homing by *Bif-1* deficiency.

In summary, the results of the present study have important implications for the prevention and treatment of cancer because they offer novel insight into the role of mitophagy in cell survival, chromosomal integrity, and evasion of apoptosis during Myc-driven malignant transformation of hematopoietic cells. Our study provides an excellent model system for understanding the importance of mitochondrial quality control in embryonic development under oncogenic stress and tumor cell homing.

Acknowledgments

Authorship

Contribution: Y.T. and T.H. performed most of the experiments and analyzed the data; T.K.C. conducted the histological and immunohistochemical analyses; J.L. performed the statistical analyses; N.D., J.M.S., and Y.I. assisted with the experiments; M.M.Y. assisted with the preparation of the manuscript; S.P. assisted with maintaining the mice; and Y.T. and H.-G.W. designed the experiments, prepared the figures, and wrote the manuscript.

Conflict-of-interest disclosure: The authors declare no competing financial interests.

Correspondence: Hong-Gang Wang, Department of Pharmacology, The Pennsylvania State University, 500 University Dr, Hershey, PA 17033; e-mail: huw11@psu.edu.

References

1. Hanahan D, Weinberg RA. Hallmarks of cancer: the next generation. *Cell.* 2011;144(5):646-674.

2. Strasser A, Cory S, Adams JM. Deciphering the rules of programmed cell death to improve therapy of cancer and other diseases. *EMBO J.* 2011;30(18):3667-3683.

3. Beroukhim R, Mermel CH, Porter D, et al. The landscape of somatic copy-number alteration across human cancers. *Nature.* 2010;463(7283):899-905.

4. Amaravadi RK, Yu D, Lum JJ, et al. Autophagy inhibition enhances therapy-induced apoptosis in a Myc-induced model of lymphoma. *J Clin Invest.* 2007;117(2):326-336.

5. Guo JY, Chen HY, Mathew R, et al. Activated Ras requires autophagy to maintain oxidative metabolism and tumorigenesis. *Genes Dev.* 2011;25(5):460-470.

6. Degenhardt K, Mathew R, Beaudoin B, et al. Autophagy promotes tumor cell survival and restricts necrosis, inflammation, and tumorigenesis. *Cancer Cell.* 2006;10(1):51-64.

7. Rao R, Balusu R, Fiskus W, et al. Combination of pan-histone deacetylase inhibitor and autophagy inhibitor exerts superior efficacy against triple-negative human breast cancer cells. *Mol Cancer Ther.* 2012;11(4):973-983.

8. Maiuri MC, Tasdemir E, Criollo A, et al. Control of autophagy by oncogenes and tumor suppressor genes. *Cell Death Differ.* 2009;16(1):87-93.

9. Mizushima N, Levine B, Cuervo AM, Klionsky DJ. Autophagy fights disease through cellular self-digestion. *Nature.* 2008;451(7182):1069-1075.

10. Valentin-Vega YA, Maclean KH, Tait-Mulder J, et al. Mitochondrial dysfunction in ataxia-telangiectasia. *Blood.* 2012;119(6):1490-1500.

11. Karantza-Wadsworth V, Patel S, Kravchuk O, et al. Autophagy mitigates metabolic stress and genome damage in mammary tumorigenesis. *Genes Dev.* 2007;21(13):1621-1635.

12. Mathew R, Kongara S, Beaudoin B, et al. Autophagy suppresses tumor progression by limiting chromosomal instability. *Genes Dev.* 2007;21(11):1367-1381.

13. Takahashi Y, Meyerkord CL, Wang HG. Bif-1/

endophilin B1: a candidate for crescent driving force in autophagy. *Cell Death Differ.* 2009;16(7):947-955.

14. Knuutila S, Aalto Y, Autio K, et al. DNA copy number losses in human neoplasms. *Am J Pathol.* 1999;155(3):683-694.

15. Lee JW, Jeong EG, Soung YH, et al. Decreased expression of tumour suppressor Bax-interacting factor-1 (Bif-1), a Bax activator, in gastric carcinomas. *Pathology.* 2006;38(4):312-315.

16. Coppola D, Oliveri C, Sayegh Z, et al. Bax-interacting factor-1 expression in prostate cancer. *Clin Genitourin Cancer.* 2008;6(2):117-121.

17. Coppola D, Khalil F, Eschrich SA, Boulware D, Yeatman T, Wang HG. Down-regulation of Bax-interacting factor-1 in colorectal adenocarcinoma. *Cancer.* 2008;113(10):2665-2670.

18. Kim SY, Oh YL, Kim KM, et al. Decreased expression of Bax-interacting factor-1 (Bif-1) in invasive urinary bladder and gallbladder cancers. *Pathology.* 2008;40(6):553-557.

19. Coppola D, Helm J, Ghayouri M, Malafa MP, Wang HG. Down-regulation of Bax-interacting factor 1 in human pancreatic ductal adenocarcinoma. *Pancreas.* 2011;40(3):433-437.

20. Takahashi Y, Karbowski M, Yamaguchi H, et al. Loss of Bif-1 suppresses Bax/Bak conformational change and mitochondrial apoptosis. *Mol Cell Biol.* 2005;25(21):9369-9382.

21. Takahashi Y, Coppola D, Matsushita N, et al. Bif-1 interacts with Beclin 1 through UVRAG and regulates autophagy and tumorigenesis. *Nat Cell Biol.* 2007;9(10):1142-1151.

22. Harris AW, Pinkert CA, Crawford M, Langdon WY, Brinster RL, Adams JM. The E mu-myc transgenic mouse. A model for high-incidence spontaneous lymphoma and leukemia of early B cells. *J Exp Med.* 1988;167(2):353-371.

23. Eischen CM, Weber JD, Roussel MF, Sherr CJ, Cleveland JL. Disruption of the ARF-Mdm2-p53 tumor suppressor pathway in Myc-induced lymphomagenesis. *Genes Dev.* 1999;13(20):2658-2669.

24. Eischen CM, Woo D, Roussel MF, Cleveland JL. Apoptosis triggered by Myc-induced suppression

of Bcl-X(L) or Bcl-2 is bypassed during lymphomagenesis. *Mol Cell Biol.* 2001;21(15):5063-5070.

25. Wong AS, Lee RH, Cheung AY, et al. Cdk5-mediated phosphorylation of endophilin B1 is required for induced autophagy in models of Parkinson's disease. *Nat Cell Biol.* 2011;13(5):568-579.

26. Takahashi Y, Meyerkord CL, Hori T, et al. Bif-1 regulates Atg9 trafficking by mediating the fission of Golgi membranes during autophagy. *Autophagy.* 2011;7(1):61-73.

27. Tsuneoka M, Umata T, Kimura H, et al. c-myc induces autophagy in rat 3Y1 fibroblast cells. *Cell Struct Funct.* 2003;28(3):195-204.

28. Langdon WY, Harris AW, Cory S, Adams JM. The c-myc oncogene perturbs B lymphocyte development in E-mu-myc transgenic mice. *Cell.* 1986;47(1):11-18.

29. White E, DiPaola RS. The double-edged sword of autophagy modulation in cancer. *Clin Cancer Res.* 2009;15(17):5308-5316.

30. Youle RJ, Narendra DP. Mechanisms of mitophagy. *Nat Rev Mol Cell Biol.* 2011;12(1):9-14.

31. Narendra D, Tanaka A, Suen DF, Youle RJ. Parkin is recruited selectively to impaired mitochondria and promotes their autophagy. *J Cell Biol.* 2008;183(5):795-803.

32. Yoshii SR, Kishi C, Ishihara N, Mizushima N. Parkin mediates proteasome-dependent protein degradation and rupture of the outer mitochondrial membrane. *J Biol Chem.* 2011;286(22):19630-19640.

33. Chan NC, Salazar AM, Pham AH, et al. Broad activation of the ubiquitin-proteasome system by Parkin is critical for mitophagy. *Hum Mol Genet.* 2011;20(9):1726-1737.

34. Tanaka A, Cleland MM, Xu S, et al. Proteasome and p97 mediate mitophagy and degradation of mitofusins induced by Parkin. *J Cell Biol.* 2010;191(7):1367-1380.

35. Karbowski M, Jeong SY, Youle RJ. Endophilin B1 is required for the maintenance of mitochondrial morphology. *J Cell Biol.* 2004;166(7):1027-1039.

36. Xie Z, Klionsky DJ. Autophagosome formation: core machinery and adaptations. *Nat Cell Biol.* 2007;9(10):1102-1109.

37. Mizushima N, Yoshimori T, Ohsumi Y. The role of Atg proteins in autophagosome formation. *Annu Rev Cell Dev Biol.* 2011;27:107-132.

38. Cuddeback SM, Yamaguchi H, Komatsu K, et al. Molecular cloning and characterization of Bif-1: A novel SH3 domain- containing protein that associates with Bax. *J Biol Chem.* 2001;276(23): 20559-20565.

39. Eischen CM, Roussel MF, Korsmeyer SJ, Cleveland JL. Bax loss impairs Myc-induced apoptosis and circumvents the selection of p53 mutations during Myc-mediated lymphomagenesis. *Mol Cell Biol.* 2001;21(22):7653-7662.

40. Zhao Z, Oh S, Li D, et al. A dual role for UVRAG in maintaining chromosomal stability independent of autophagy. *Dev Cell.* 2012;22(5):1001-1016.

41. Liang C, Feng P, Ku B, et al. Autophagic and tumour suppressor activity of a novel Beclin1-binding protein UVRAG. *Nat Cell Biol.* 2006;8(7):688-699.

42. Liang C, Lee JS, Inn KS, et al. Beclin1-binding UVRAG targets the class C Vps complex to coordinate autophagosome maturation and endocytic trafficking. *Nat Cell Biol.* 2008;10(7):776-787.

43. Hayashi-Nishino M, Fujita N, Noda T, Yamaguchi A, Yoshimori T, Yamamoto A. A subdomain of the endoplasmic reticulum forms a cradle for autophagosome formation. *Nat Cell Biol.* 2009; 11(12):1433-1437.

44. Yla-Anttila P, Vihinen H, Jokitalo E, Eskelinen EL. 3D tomography reveals connections between the phagophore and endoplasmic reticulum. *Autophagy.* 2009;5(8):1180-1185.

45. Campbell KJ, Bath ML, Turner ML, et al. Elevated Mcl-1 perturbs lymphopoiesis, promotes transformation of hematopoietic stem/progenitor cells, and enhances drug resistance. *Blood.* 2010; 116(17):3197-3207.